Calculation of Pressure in Ocean Simulations

WILLIAM K. DEWAR AND YA HSUEH

Department of Oceanography, The Florida State University, Tallahassee, Florida

TREVOR J. MCDOUGALL

CSIRO Division of Marine Research, Hobart, Australia

DONGLIANG YUAN

Department of Oceanography, The Florida State University, Tallahassee, Florida

(Manuscript received 25 June 1996, in final form 30 June 1997)

ABSTRACT

Many state-of-the-art numerical ocean models calculate pressure using the hydrostatic balance, or an equation derived from it. The proper form of this deceptively simple-looking equation, $\partial p/\partial z = -g\rho(S, T, p)$ (where notation is standard), is nonlinear in the pressure p. In contrast, most numerical models solve the linear equation $\partial p/\partial z = -g\rho(S, T, z)$. This modification essentially replaces the total pressure, which includes a time-dependent signal, with an approximate time-independent pressure associated with the depth of a model grid point. In this paper, the authors argue that the inclusion of the total pressure when solving the hydrostatic equation can generate a depth-dependent baroclinic pressure gradient equivalent to a geostrophic velocity of several centimeters per second. Further, this effective velocity can increase with depth and is largest in dynamically important areas like western boundary currents. These points suggest that the full feedback of pressure on density should be included in numerical models. Examples of the effect using oceanic data and output from a typical primitive equation model run are discussed. Finally, algorithms for both rigid-lid and free surface models that explicitly include full pressure are derived, and some related numerical issues are discussed.

1. Introduction

Numerical modeling of the ocean is often performed using the so-called primitive equations, consisting of horizontal momentum equations, the continuity equation, conservation equations for salt and potential temperature, the hydrostatic equation

$$\frac{\partial p}{\partial z} = -g\rho(S, T, p), \tag{1.1}$$

and an equation of state.[1] The commonly accepted standard for the latter is the UNESCO state equation, which expresses density (ρ) as a function of temperature (T), salinity (S), and pressure (p) (Millero et al. 1980). Other choices for the equation of state have appeared recently (Jackett and McDougall 1995; Feistel 1993; Feistel and Hagen 1995), all of which employ pressure as an independent variable. The form of the equation of state renders (1.1) a nonlinear differential equation for pressure. In contrast, numerical models often solve a modified form of (1.1), that is,

$$\frac{\partial p}{\partial z} = -g\rho(S, T, z), \tag{1.2}$$

which is a linear equation. As numerical models strive for accuracy in the simulation of modern-day climate, it is essential that classical approximations be reassessed for their accuracy. The objectives of this paper are to consider the impacts of the above approximation and to outline procedures for improving models by employing (1.1).

Background

The rationale for the use of (1.2) instead of (1.1) is that total pressure and static pressure differ by a relatively small amount, so depth may be substituted for

[1] A slight inconsistency appears in the above discussion, in that a conservation equation for potential temperature is mentioned, but an equation of state depending on in situ temperature is listed. This can be remedied by using the Jackett and McDougall (1995) equation of state, but as the distinction between potential and in situ temperature is not central to our message, we will refer simply to a temperature variable T in what follows.

Corresponding author address: Dr. William K. Dewar, Department of Oceanography, The Florida State University, Tallahassee, FL 32306.
E-mail: bill@ocean.ocean.fsu.edu

pressure using a routine like that proposed by Fofonoff and Millard (1983).[2] Thus, for example, in Cartesian and bottom following (sigma) coordinate models, where grid points are fixed in space, the depth of a grid point is equated to a pressure, which is subsequently time independent. This ''pressure'' is then fed through the model equation of state along with current T and S values to arrive at a density. Equation (1.2) is then integrated from the surface into the interior. The resulting pressure field, when differenced, provides a ''baroclinic'' acceleration to the momentum equations.

Calculation of the remaining model external, or surface, pressure is done either by explicit calculation of the free surface or the diagnosis of surface pressure via a rigid-lid assumption. Relative to the former method, Killworth et al. (1991) solve an explicit equation for free surface elevation using small time steps relative to those used for the baroclinic fields. In contrast, Dukowicz and Smith (1994) use an implicit scheme in which the external and internal equations use the same time step. Relative to the latter method, the vertically integrated momentum equations are manipulated to yield an equation either for a barotropic streamfunction or for surface pressure. In the streamfunction case, ''baroclinic'' velocities are predicted from the momentum equations and adjusted to yield a net transport consistent with the streamfunction. In the surface pressure case, an acceleration term proportional to the surface pressure gradient is added to the momentum equations, and full velocity is predicted. Total horizontal velocities, T, and S fields are then known and the model is prepared to advance in time.

Implicit in these integration schemes is the assumption that the difference between the total pressure and an approximate fixed pressure at a given depth has a negligible impact on density, and can be ignored. This appears in the use of a depth-based equation of state and in the diagnosis of surface pressure, which assumes a priori knowledge of the density field. The disparity between the small dynamically generated pressure signals characteristic of the open ocean [O(1 dbar)] and the enormous nearly static pressures in the ocean interior (thousands of dbars) supports this as a rational and accurate approximation. Indeed, we do not take exception to this point. The correction density induced by total pressure variability is tiny and comparable to the uncertainty in density currently introduced by measurement error in temperature and salinity. However, whereas the measurement errors are random, the replacement of pressure by depth in the equation of state can introduce a systematic bias in the calculation of density. Further, to calculate pressure, the small and often monotonic, density corrections are multiplied by gravity and integrated over large depths.

Here we argue by means of a simple scale analysis that the above contribution to the baroclinic pressure is sizeable. When converted to an equivalent geostrophic velocity, it can be several centimeters per second in size. Further, we present some explicit examples, using data from the Gulf Stream region and from numerical models, of the types and magnitudes of the pressure corrections. Thus, we suggest that models should include the implicit dependence of density on pressure, that is, use (1.1) instead of (1.2). Finally, we outline procedures by which this may be accomplished.

2. Scale arguments

The simplest example of the importance of total pressure in the equation of state involves surface pressure. Consider an ocean stratified in temperature and salinity, but assume the T and S fields are perfectly flat (see Fig. 1a). This assumption, while not oceanically realistic, allows us to focus solely on the baroclinic effect of external pressure gradients.

Pressure will be calculated at the two hydrocasts denoted A and B in Fig. 1a, which are assumed to be 50 km apart, that is, at a spacing characteristic of many open ocean sections and coarse resolution numerical models. Equation (1.1) must be integrated to obtain pressure, and this may be accomplished by a number of techniques (e.g., a Runge–Kutta method). The result, shown implicitly, is

$$p(z) = p_s + g \int_z^o \rho \, dz, \tag{2.1}$$

where we have employed a rigid-lid approximation and p_s denotes surface pressure (at $z = 0$).[3] The dynamically important pressure gradient may be calculated from (2.1); namely,

$$\frac{\partial p}{\partial x} = \frac{\partial p_s}{\partial x} + g \int_z^o \frac{\partial \rho}{\partial x} \, dz. \tag{2.2}$$

Thus, the internal pressure gradient is due to the familiar surface contribution and to what is normally termed the baroclinic contribution. The T, S structure described above and shown in Fig. 1a suggests that the latter vanishes, or at least ρ_x is vanishingly small. However, upon using the equation of state, the integrand in (2.2) is

$$\frac{\partial \rho}{\partial x} = \rho(-\alpha\theta_x + \beta S_x) + \rho_p p_x = \frac{p_x}{c_s^2}, \tag{2.3}$$

where α and β are the thermal expansion and saline

[2] The inclusion of pressure in the equation of state does not violate the usual Boussinesq filtering of sound waves. This is assured by the neglect of a time derivative in the continuity equation. What is retained here is the slow time and space scale density variability caused by pressure.

[3] We neglect the atmospheric contribution to surface pressure in this paper. Since gradients of pressure are what matters, this is equivalent to assuming a spatially uniform atmospheric pressure.

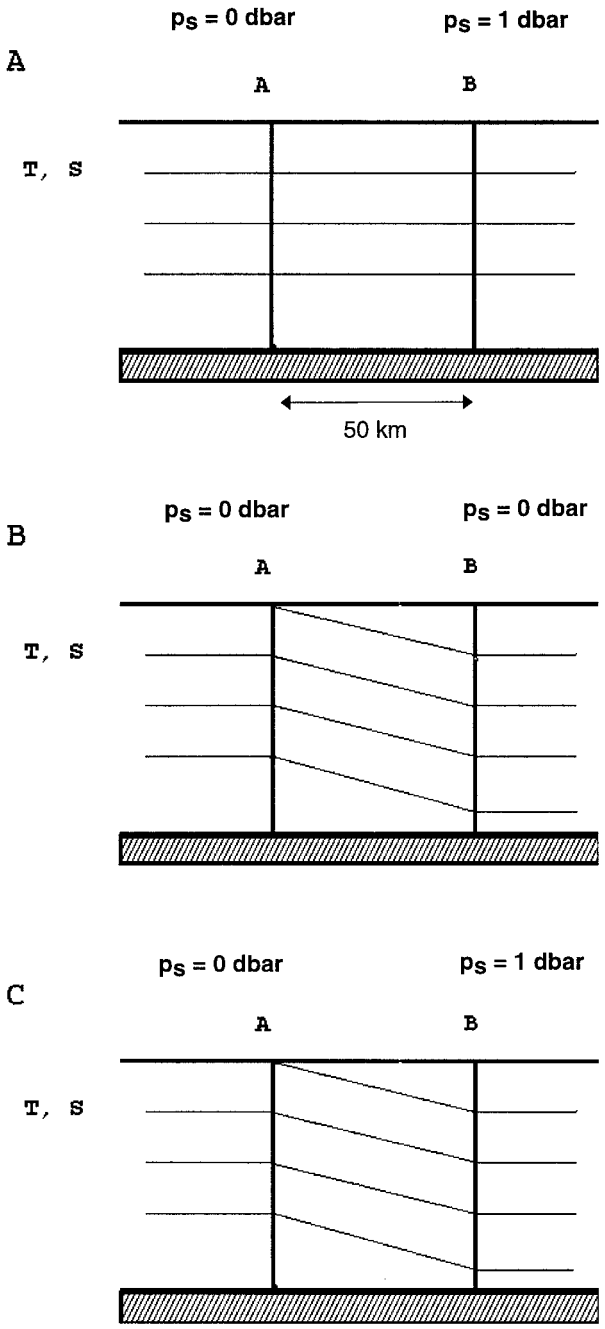

FIG. 1. Scale argument schematics. In (a), it is assumed the T and S fields are perfectly flat between two stations, A and B, situated 50 km apart. A rigid lid is employed but the surface pressure at station A is assumed to differ from that at B by 1 dbar, that is, roughly the surface pressure difference across the Gulf Stream. In (b), the surface pressure gradient is assumed to vanish, but the interior T and S surfaces are not flat. In (c), gradients of surface pressure, T, and S exist.

contraction coefficients of seawater; subscripts p and x denote differentiation; the p derivative of ρ, ρ_p, is taken at constant T and S; and c_s denotes sound speed. Also, we have employed the assumed tracer structure of Fig. 1a to arrive at the final formula in (2.3). Thus, it is seen that even in the case of perfectly flat tracer fields, a ''baroclinic'' contribution to the pressure gradient still can exist. This contribution comes from the pressure dependence of density and, in the present case, finds its origins in surface pressure gradients. In contrast, the density gradient in (2.3) would vanish if the depth-based equation of state in (1.2) were used.

A difficulty of using (2.3) in (2.2) is the appearance of the pressure gradient on both sides of the equation. However, (2.3) may be employed on the right-hand side of (2.2) to estimate the size of the baroclinic contribution to the left-hand side. The pressure gradient on the right-hand side of (2.3) is at least as large as the surface pressure gradient. Surface pressure differences across the Gulf Stream can be as great as 1 dbar for a 50 km separation; thus we approximate p_x by

$$p_x \approx \left[\frac{10^4 \ \frac{\text{kg}}{\text{m s}^2}}{5 \times 10^4 \text{ m}}\right] \approx 0.2 \frac{\text{kg}}{\text{m}^2 \text{ s}^2}. \tag{2.4}$$

Using a sound speed of 1500 m s^{-1} and a gravitational acceleration of 10 m s^{-2}, the baroclinic contribution to (2.2) at a depth of $H = 1$ km is roughly

$$p_x \approx \frac{g p_{sx} H}{c_s^2} \approx \frac{10 \text{ m}}{\text{s}^2}\left(0.2 \frac{\text{kg}}{\text{m}^2 \text{ s}^2}\right)(10^3 \text{ m})\left(1500 \frac{\text{m}}{\text{s}}\right)^{-2}$$

$$\approx 10^{-3} \frac{\text{kg}}{\text{m}^2 \text{ s}^2}. \tag{2.5}$$

If we now assume that the basic momentum balance is geostrophic, the above can be converted to an equivalent velocity; that is,

$$v \approx \frac{g H p_{sx}}{c_s^2 \rho f} \approx 0.01 \frac{\text{m}}{\text{s}}. \tag{2.6}$$

Thus, we see that the effect on density of a Gulf Stream–like surface pressure integrates roughly to a current of 1 cm s^{-1} at a depth of 1 km. Several further points about this should also be made. First, this effect is roughly proportional to depth. Thus, we may expect at depths of 5 km (typical of those under the Gulf Stream at 63°W), the equivalent velocity will be more like 5 cm s^{-1}. Second, this baroclinic contribution to pressure augments the surface pressure gradient, a result due to the positive feedback between high pressures and high densities in the equation of state. A result of this is that the neglect of surface pressure in the equation of state underestimates downstream transport. Third, assuming a scale velocity of 2 cm s^{-1} throughout the lower 4 km of a Gulf Stream–like current, the transport due to the above effect is 4 Sv (Sv $\equiv 10^6$ m^3 s^{-1}). For comparison, this is roughly 1% of the transport implied by the structure in Fig. 1a. On the other hand, 4 Sv represents approximately 25% of the estimated 15 Sv thermohaline transport of the North Atlantic (Dickson et al. 1990). Finally, this extra velocity is missed if (1.2) is used

because a depth-based equation of state cannot react to a dynamically generated pressure signal.

a. Internal pressure effects

Now consider the opposite case of no surface pressure gradients, but large horizontal gradients in T and S (see Fig. 1b). In this case, all the terms in (2.3) must be retained, while the surface gradient in (2.2) can be ignored. We again appeal to a Gulf Stream–like case to estimate the impact of the compressibility in (2.2). Here, temperature differences of 5°C can occur over 50 km (Rossby 1984). Characterizing the upper 1000 m by this value, using $\alpha = 2 \times 10^{-4}$ K^{-1} and neglecting any salinity contributions, yields an estimate of the net pressure change at a depth of 1000 m of

$$\Delta p = g \int_z^o \rho(-\alpha \Delta\theta)\, dz$$

$$\approx \frac{10 \text{ m}}{\text{s}^2}\, 1000 \text{ m}\, \frac{1000 \text{ kg}}{\text{m}^3}\, \frac{2 \times 10^{-4}}{\text{K}} 5 \text{ K} \approx 1 \text{ dbar}. \tag{2.7}$$

The contribution to the pressure gradient due to the compressibility [i.e., the last term in (2.3)] results from an integral of the pressure gradient over the upper kilometer, which itself has been accruing due to the temperature structure. The effect of the last term in (2.3) is thus estimated using the average of the vanishing surface pressure gradient and the 1 dbar difference at 1 km; that is,

$$v = \frac{g}{\rho f} \int_z^o \frac{p_x}{c_s^2}\, dz$$

$$\approx \frac{10 \text{ m}}{\text{s}^2}\, \frac{1000 \text{ m}}{1000 \text{ kg m}^{-3}\ 10^{-4} \text{ s}^{-1}}$$

$$\times \frac{\frac{10^4}{2}\, \frac{\text{kg}}{\text{m s}^2}}{5 \times 10^4 \text{ m } 2.25 \times 10^6 \text{ m}^2 \text{ s}^{-2}} \approx .005\, \frac{\text{m}}{\text{s}}, \tag{2.8}$$

that is, 5 mm (s^{-1}). A velocity of this size over a water column 50 km wide by 5 km deep yields a 1-Sv transport.

b. Combined surface and internal pressure gradients

It is often the case that surface pressure gradients and internal T and S fields conspire against each other so as to reduce the magnitude of the deep pressure gradients (see Fig. 1c). Such is the case in all subtropical western boundary currents, where the presence of a relatively light water mass in the offshore gyre offsets the relatively high offshore surface pressure head. It is worth pointing out explicitly that the estimate (2.8) applies also to this situation. To see this, we note that the above baroclinic pressure gradient contribution in the presence of the Gulf Stream surface pressure is just sufficient to cancel the surface pressure at a depth of 1 km. Again, to estimate the contribution to the pressure gradient from the compressibility term, an average of the surface and 1-km pressure gradients should be used. The result is thus identical to (2.8).

c. Comparisons with other density errors

To provide context and to offer an explanation of this effect, the contribution to density caused by surface pressure is here compared to those caused by measurement errors. We will assume a thermal expansion coefficient of 2×10^{-4} K^{-1} and a saline contraction coefficient of 8×10^{-4}/psu (Gill 1982).

The typical uncertainty associated with modern CTDs is roughly ± 0.002 psu for salinity, and ± 0.002 K for temperature (WOCE Operations Manual 1994). These translate into a relative density error of $\pm 4(16) \times 10^{-7}$ for temperature (salinity), or roughly $\pm 4(16) \times 10^{-4}$ kg m^{-3}. In comparison, an error of 1 dbar in pressure yields a slightly larger error in density, that is, 4×10^{-3} kg m^{-3}. So it is seen that the correction to density caused by surface pressure is tiny and comparable to the unavoidable uncertainty in density due to measurement error. However, in contrast to measurement error, the pressure contribution is systematic. While salinity and temperature measurement errors can be expected to average themselves out, the pressure contribution is persistent. It is principally for this reason that pressure feedback ultimately yields a sizeable extra velocity. Also, this effect occurs in numerical models, where perfect accuracy in the measurement of T and S can be claimed.

3. Some oceanic examples

We now explore the impact of total pressure on velocity using oceanic data. We have selected profiles of temperature and salinity from the Levitus North Atlantic dataset (Levitus 1982). A standard fourth-order Runge–Kutta integration method was then used to solve the hydrostatic equation (1.1), subject to a surface pressure condition and the UNESCO equation of state.

A plot of difference in pressure versus depth generated by two such integrations appears in Fig. 2. Here we have used a Levitus cast from the Sargasso Sea, specifically at (33.5°N, 69.5°W). The integrations differ only in their respective surface pressures; one assumes a surface pressure of 0 dbars, and the other a surface pressure of 1 dbar. Equivalently, the pressure fields generated here would be like those generated from the casts in Fig. 1a. Also in Fig. 2, a vertical profile of the equivalent geostrophic velocity associated with the pressure differences appears. Here, we have assumed a horizontal separation of 50 km and used the Coriolis parameter relevant to 33.5°N. The results quantify and support the scaling argument that appeared in section 1. Velocities

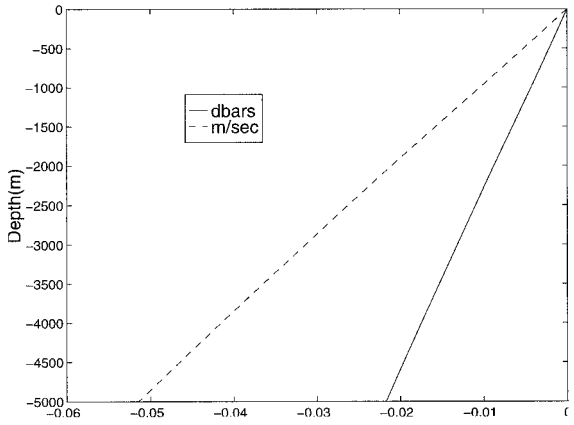

FIG. 2. Hydrostatic pressure difference versus depth from a station in the Sargasso Sea. The temperature and salinity structure is identical for the two integrations of the hydrostatic equation. The displayed difference is due to an initial surface pressure difference of 1 dbar. Also shown is the equivalent geostrophic velocity implied by the pressure difference.

of several centimeters per second are seen as one proceeds down the water column.

Perhaps of more interest are the comparisons shown in Fig. 3. Here, we have again selected *T* and *S* profiles from the Levitus North Atlantic dataset. However, in this case, the profiles come from the climatological path of the Gulf Stream. Specifically, the locations of the casts are (42.5°N, 59.5°W) and (39.5°N, 59.5°W). Thus, in this comparison, the lateral *T* and *S* structure of the Gulf Stream generates the major portion of the internal baroclinic pressure gradient. We compare the equivalent geostrophic velocities generated by two sets of calculations. In both sets, the offshore profile was assigned higher surface pressures characteristic of the Gulf Stream, while the inshore profile was assigned a vanishing surface pressure value. The calculations differ in that in the first set, surface pressure was neglected as an effect on subsurface density, while it was included as an effect in the second set. The section-averaged Coriolis parameter (at 41°N) and section-averaged density were then used to convert the pressure gradient to a geostrophic velocity. The data from the northern location went only to a depth of 3.5 km, while the southern cast extended to 5 km. The northern cast was therefore artificially deepened to 5 km by filling in the bottom 1.5 km with the data from the southern cast.

First a word about the resulting ''Gulf Stream'' profiles is in order. A typical surface pressure change across the Gulf Stream is 1 dbar, and the surface velocities associated with this are roughly 0.33 m s^{-1}. Indeed, these seem reasonable for a climatological Gulf Stream. In contrast, the diagnosed bottom velocities for this surface pressure difference are large, roughly 0.19 m s^{-1}. The corresponding transport (roughly 330 Sv) is therefore too large by a factor between 2 and 3 when compared to the real Gulf Stream. We have therefore also calculated velocity profiles with smaller surface pres-

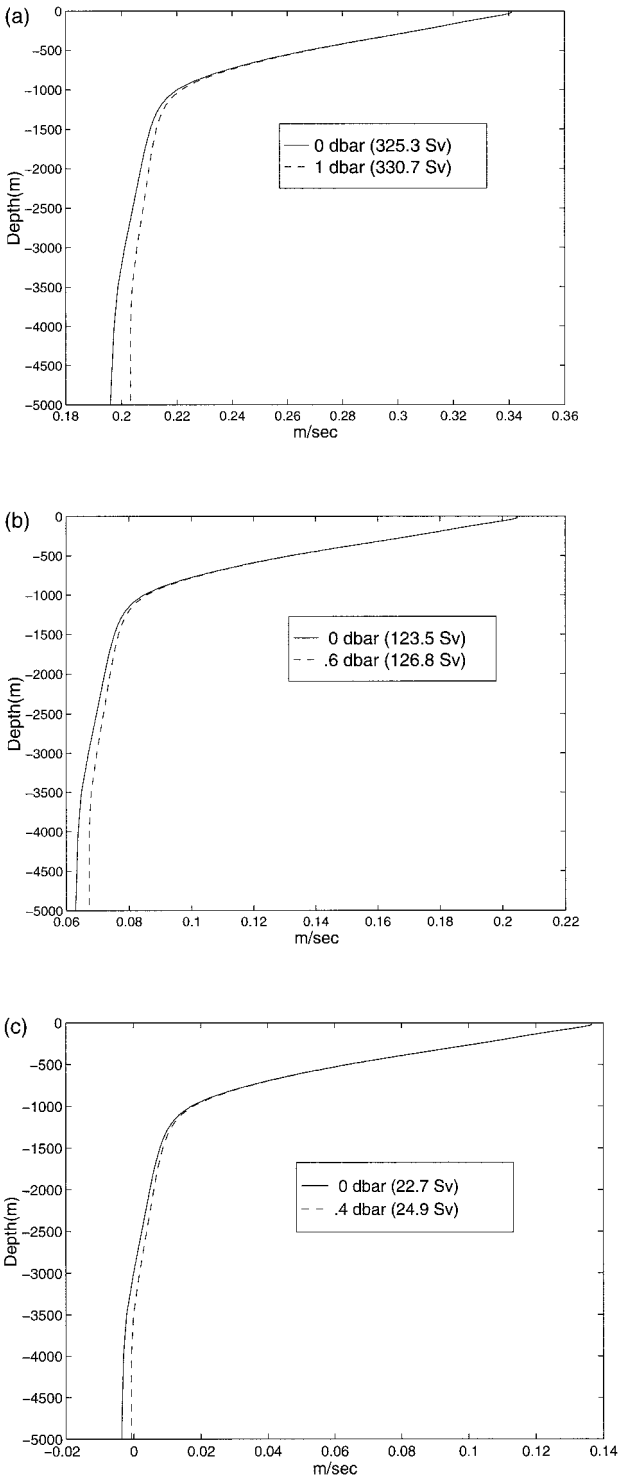

FIG. 3. Gulf Stream velocities. The *T* and *S* data were obtained from hydrocasts located within the climatological Gulf Stream path and pressure was calculated using the hydrostatic equation. In one case, labeled ''0 dbars'' in (a), (b), and (c), surface pressure was neglected as an effect on density. In the other case, labeled ''1 dbar'' in (a) ''0.6 dbar'' in (b), and ''0.4 dbar'' in (c), surface pressure was included in the calculation of density. The two traces in each plot are of the implied geostrophic velocity profiles. Total transport for each profile appears in the legend.

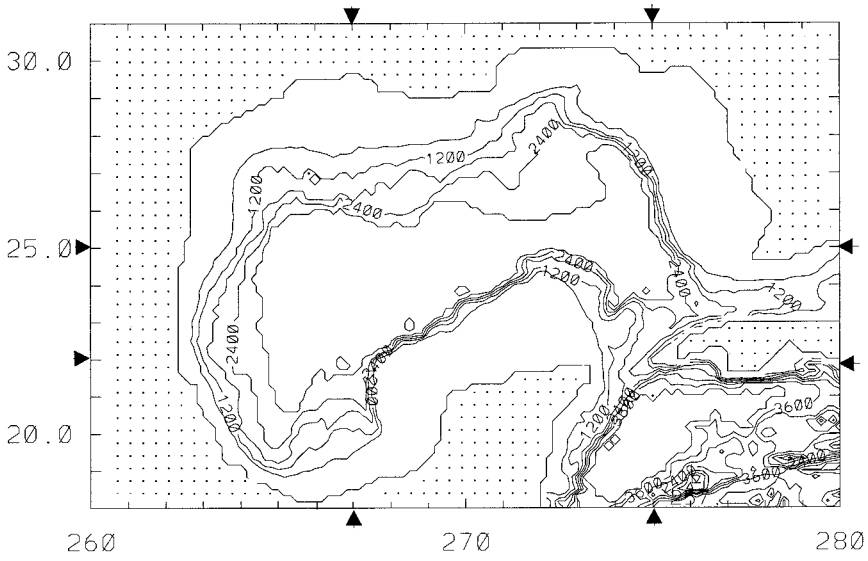

FIG. 4. The Gulf of Mexico domain and bottom topography used in the Bryan–Cox model. The arrows indicate the sections on which transports have been calculated. Contours of depth in meters, contour interval 600 m.

sures in order to achieve a more representative Gulf Stream transport. For example, we have experimented with $\Delta p_s = 0.6$ dbars and $\Delta p_s = 0.4$ dbars. The former value, although small for the Gulf Stream, yields a reasonable transport of 125 Sv. Associated with this are surface velocities of 0.20 and 0.06 m s^{-1} bottom velocities. The latter value results in a weak total transport of 25 Sv, surface velocities of 0.13 m s^{-1}, and a reversal in sign of the bottom flow (~ -0.004 m s^{-1}). We have computed velocity profiles with and without compressibility for both of these net surface pressure changes, with the idea that the results give upper and lower bounds on the magnitude of the effect.

The velocity differential for $\Delta p_s = 1$ dbar is shown in Fig. 3a; note at a depth of 5000 m the value is roughly 0.8 cm s^{-1}. This relatively small value is due mostly to the large spacing between the hydrocasts (300 km). Nonetheless, the calculation recognizing the contribution of surface pressure possesses the larger deep velocities. Although the velocity difference is rather modest, net transport depends only on the pressure differential. We have also compared the section transports from these two calculations, and find an increased transport of 5.4 Sv for the section in which surface pressure was used to compute density. In view of the anomalously large total transport of this section, we consider this to be a upper bound. Velocities for the case of $\Delta p_s = 0.6$ dbar appear in Fig. 3b. Computing section transports from the profiles yields a difference of 3.3 Sv with the calculation involving surface pressure possessing the larger transport. The transport differential in the limit of small Gulf Stream transports is not very sensitive to the surface pressure. For example, the experiment with $\Delta p_s = 0.4$ dbar shown in Fig. 3c yields a transport difference in excess of 2 Sv. (Note, the reversal in velocity mentioned above characterizes the lower 1500 m of the velocity profile.) Therefore, we suggest 3 Sv as a rough lower bound on the size of the feedback effect for the Gulf Stream.

4. An example from a numerical model

Next, we consider output from a numerical model in order to examine the impact of compressibility on pressure. Specifically, we use a version of the Bryan–Cox model customized to the Gulf of Mexico. The domain and bottom topography appears in plan view in Fig. 4.

The model has a horizontal resolution of 1/6 degree in both latitude and longitude and 25 levels in the vertical. The southern (at 18°N) and eastern (at azimuth angle 280°E, i.e., 80°W) boundaries are ''open'' in that flow is permitted to cross them.

Net transport in the Bryan–Cox model is governed by a barotropic streamfunction. This was initialized by adjusting the streamfunction boundary conditions over a period of two model months from a state of no inflow to one in which an inflow of 30 Sv occurred in a 100-km strip against the Yucatan Peninsula. This flow was conducted out of the domain through the model boundary north of Cuba. The model was run in a purely barotropic mode for this purpose (this reduces to solving an elliptic equation for the streamfunction). The subsurface T and S fields were then initialized using the annual mean climatology of Levitus et al. (1994a, b), and the velocity was determined geostrophically using the thermal wind relationship in conjunction with the streamfunction.

We will discuss here the results of a 90-day integration. Surface T and S were relaxed during the model

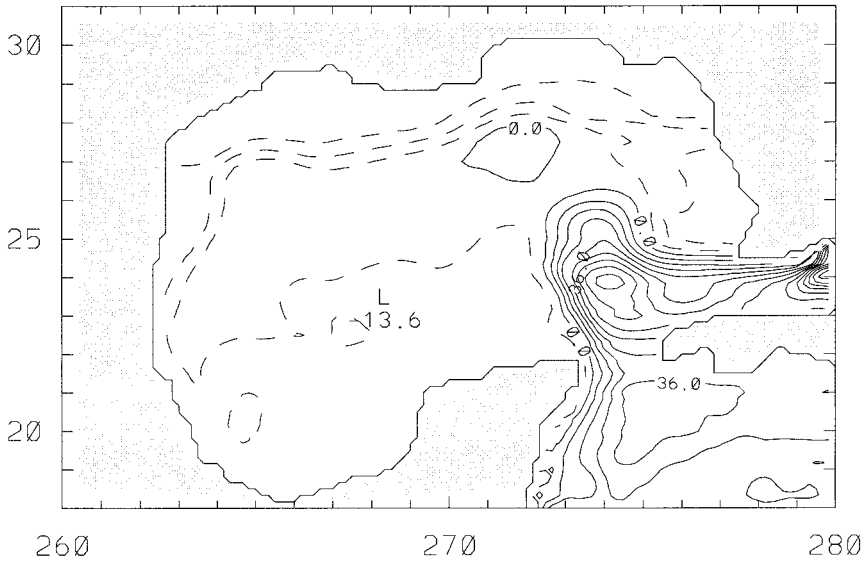

FIG. 5. Sea surface height in centimeters, diagnosed from our Bryan–Cox Gulf of Mexico model, after 90 days of integration. Contours from −27 to 117 cm, contour interval of 9 cm.

run toward Levitus Gulf of Mexico climatology with a relaxation timescale of 50 days. At inflow points at the domain boundary, the subsurface T and S fields were relaxed toward Levitus climatology. The five grid points neighboring the boundary accomplished this by means of a buffer zone. The relaxation timescales in this zone increase from a minimum of a few hours at the boundary to a maximum of roughly 1/2 day at the outer edge of the buffer. Further, at the 30-Sv inflow point, the subsurface velocities are relaxed toward the thermal wind profile consistent with the Levitus climatology. A radiation condition on T and S is used on the boundary at points of outflow. This procedure is essentially that used in several recent regional modeling studies of the western Pacific marginal seas (Schultz 1994; Hsueh 1997, manuscript submitted to *J. Mar. Syst.*; Hsueh et al. 1997, manuscript submitted *Progr. Oceanogr.*). Finally, no wind stress forcing has been used to generate the results discussed here.

The Bryan–Cox model predicts ''baroclinic'' velocities by time stepping the momentum equations with the pressures obtained by integrating (1.2). These baroclinic velocities are subsequently adjusted to produce a net transport consistent with the streamfunction.

The difference between the baroclinic and total velocities is due to acceleration in the momentum equations caused by the surface pressure gradient. Thus, this gradient is easily diagnosed given model velocity, temperature, and salinity output from two adjacent time levels. As we need surface pressure to compute the effects of compressibility, we chose a point within the model Gulf of Mexico and used our diagnosed surface pressure gradients to compute surface pressure everywhere.

The effective sea surface height field at 90 days as diagnosed by the above procedure is shown in Fig. 5. The major feature seen in this field is, not surprisingly, the Loop Current entering in the Yucatan and exiting at the Florida Straits. In this particular run, the Loop Current and the remainder of the Gulf of Mexico are devoid of Loop Current rings. The model temperature and salinity fields at this point in the integration were analyzed.

We next computed two sets of subsurface pressures in a manner analogous to that described in the previous section. Namely, a Runge–Kutta method was used to solve (1.1) subject to an initial condition of 0 dbar at $z = 0$ m. The Jackett and McDougall (1995) equation of state, depending on potential temperature, salinity, and pressure, was used. When the results are added to the surface pressure, a total pressure versus depth curve at each grid point is obtained. This field was then finite differenced and converted to a geostrophic velocity in the standard way. This procedure was then repeated except surface pressure was used to initialize the Runge–Kutta integration. The second geostrophic velocity estimate was then subtracted from the first, and the results plotted on the model depth levels.

Velocity difference on model level 20 (depth 1787 m) appears in Fig. 6. Vectors representing fluid speed and direction are plotted at every second model grid point. The maximum vector in this diagram occurs in the area of the Loop Current and is 0.95 cm s^{-1}, which agrees well with the scale estimate obtained in section 2. In fact, this characterizes the size of the velocity differential throughout the area of the Loop Current. Away from this energetic feature, the magnitudes drop considerably, so that in the western Gulf of Mexico the vectors represent differencences more like 0.01 cm s^{-1}.

Deeper levels are not shown because there is not much area in the Gulf of Mexico at depths greater than about 2000 m. In addition, the Loop Current largely disappears

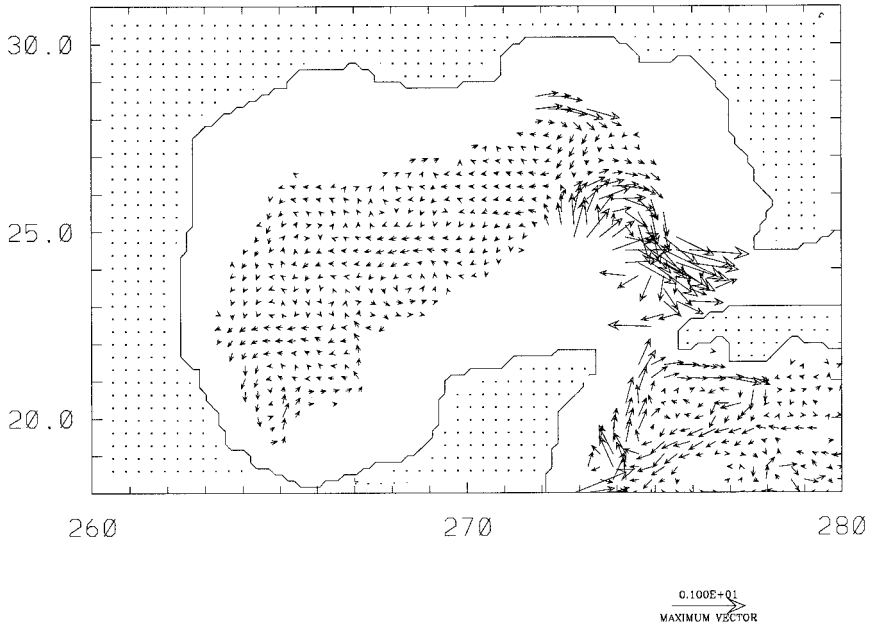

FIG. 6. Velocity difference vectors at model level 20 (depth 1787 m). The difference here is due to the inclusion of surface pressure in the calculation of density.

at greater depth levels, due to its path lying over the shallower parts of the model. Therefore, in the small areas present at deep levels, the velocity differences are usually no larger than 0.1 cm s^{-1}.

We have also computed transports across various Gulf of Mexico sections. These sections are indicated by the arrows in Fig. 4. As the Gulf of Mexico is almost a closed body of water, the net transport across several of these sections must vanish. We therefore segregated the transport calculation by sign, and quote here only the positive transports (i.e., either the northward or eastward transports). These results appear in Table 1, from which it can be seen that the transport differences range from 3 Sv for sections involving the Loop Current to roughly 0.3 Sv away from the Loop Current.

We hasten to add that we are computing a difference here between the ''correct'' pressure and an ''approximate'' pressure, which is more accurate than the pressure normally computed by the model. The reason for this is that we solve (1.1) to obtain both pressure fields, while the Bryan–Cox model uses (1.2), that is, the model neglects all pressure feedbacks in computing density. The difference in the pressure fields (expressed in terms of geostrophic velocity) appearing in Fig. 6 is caused only by the neglect of surface pressure in one of our integrations. The pressure field as normally computed by the Bryan–Cox model neglects not only this effect on density, but also that due to the effects of a dynamically depth-varying pressure on density.

TABLE 1. Transport anomalies across various sections in the Gulf of Mexico model. Positive geostrophic velocity differences were summed on the indicated meridional and zonal transects to given the anomalous tranports. The locations of the transects are indicated by the arrows in Fig. 4.

Orientation	Location	Transport (Sv)
Zonal	22°N	.35
Zonal	25°N	1.8
Meridional	267°E (93°W)	1.8
Meridional	275°E (85°W)	3.0

5. Recommendations

We feel these results show that it is adviseable to allow for dynamic pressure effects in the calculation of interior pressure gradients in ocean models. On the other hand, to do so requires a reworking of the integration procedures. At the heart of the problem is the use of a depth-based equation of state. Such a procedure implicitly assumes that pressure is well approximated by a static field; however, we have argued that differences of O(3 Sv) in transport can occur when variable total pressure is accounted for.

We now outline procedures for both rigid lid and free surface models that explicitly include the real equation of state and its dependence on total pressure. The salient equations in both cases are

$$\rho_o u_t = -p_x + f^{(x)} \tag{5.1a}$$

$$\rho_o v_t = -p_y + f^{(y)} \tag{5.1b}$$

$$p_z = -g\rho(S, T, p) \tag{5.1c}$$

$$u_x + v_y + w_z = 0, \tag{5.1d}$$

where $f^{(x)}$ and $f^{(y)}$ denote the nonlinear, Coriolis, and viscous terms of the zonal and meridional momentum equations, respectively, and other notation is standard.

One issue common to both model types is the solution of (5.1c). For this we recommend the use of a Runge–Kutta (RK) method. The main computational cost here, normally due to the several evaluations of the equation of state inherent in the RK method, can be controlled through the use of a polynomial equation of state like those recently proposed by Feistel (1993) and Feistel and Hagan (1993, 1995).

Specifically, the problem reduces to the prediction of pressure at the next deeper depth grid point, given pressure and depth at the present grid point. The model T and S data at levels intermediate to the depth grid points are obtained by averaging neighboring T and S values. The Feistel equation of state is a polynomial in $S^{1/2}$, T, and p. The model T and S values can be used to evaluate much of this function, leaving a local state equation depending on p only (the current Feistel formula results in a fourth-order polynomial). Calculating the coefficients of this fourth-order polynomial in p represents the most significant computational load of the procedure, as the subsequent Runge–Kutta integration of the lower-order polynomial to the next depth level is straightforward.

a. Rigid-lid models

We assume that at a given time step, full horizontal velocities, surface pressure, potential temperature, and salinity are known. Classical methods are then employed to predict full velocity, potential temperature, and salinity at the next time step. What remains is to compute the updated pressure. For this, we propose a variant of the procedure that diagnoses surface pressure, rather than barotropic streamfunction. In this case, the usual manipulations of (5.1a,b), and application of the rigid-lid boundary conditions, eventually yields

$$0 = \left[\frac{\partial^2}{\partial x^2} + \frac{\partial^2}{\partial y^2}\right]\int_{-H}^{0} p\, dz + (p(-H)H_x)_x + (p(-H)H_y)_y + F_x^{(x)} + F_y^{(y)}, \tag{5.2}$$

where H is the total fluid depth and

$$F^{(x),(y)} = \int_{-H}^{0} f^{(x),(y)}\, dz.$$

For the purposes of illustration, we have used the continuous equations to obtain (5.2). We consider various discretization issues below.

If (2.1) is differentiated with respect to surface pressure, the result is

$$\frac{\partial p}{\partial p_s} = 1 + g\int_z^0 \frac{p_{p_s}}{c_s^2}\, dz. \tag{5.3}$$

An approximate solution to this integral equation for p_{p_s} is

$$p_{p_s} = 1.$$

The leading order correction to the above can therefore be found by employing it in the integral in (5.3), leading to

$$p_{p_s} \approx 1 + g\int_z^0 \frac{1}{c_s^2}\, dz = 1 - \frac{gz}{(1500\ \text{m s}^{-1})^2} = 1 + gG(z), \tag{5.4}$$

where we have used a fixed value of 1500 m s^{-1} for sound speed.

Pressure variations caused by the surface pressure are small, so density may be approximated by a Taylor expansion; that is,

$$\rho = \rho(S, \theta, p(p_s = 0) + p_{p_s}p_s) = \rho(S, \theta, p(p_s = 0)) + \frac{(1 + gG(z))}{c_s^2}p_s, \tag{5.5}$$

where $G(z) = -z/(1500\ \text{m s}^{-1})^2$ and the first term on the right-hand side can be obtained using the above Runge–Kutta methods subject to a vanishing surface pressure. Substituting (5.5) into (2.1) and writing $\rho(S, \theta, p(p_s = 0))$ as $\overline{\rho}$, we obtain

$$p = p_s(1 + gG(z)) + g\int_z^0 \overline{\rho}\, dz + O\left(\frac{g^2H^2p_s}{c_s^4}\right), \tag{5.6}$$

which may be used to get an expression for the vertically integrated pressure in terms of $\overline{\rho}$ and surface pressure. Then, substituting (5.6) in (5.2) and simplifying leads to a diagnostic equation for surface pressure:

$$0 = -\frac{\partial}{\partial x}\left[p_{s_x}\left(H + g\int_{-H}^{0} G\, dz\right)\right] - \frac{\partial}{\partial y}\left[p_{s_y}\left(H + g\int_{-H}^{0} G\, dz\right)\right] - g\left[\frac{\partial}{\partial x}\left[\int_{-H}^{0}\frac{\partial}{\partial x}\int_{-z}^{0}\overline{\rho}\, dz'\, dz\right] - \frac{\partial}{\partial y}\left[\int_{-H}^{0}\frac{\partial}{\partial y}\int_{-z}^{0}\overline{\rho}\, dz'\, dz\right]\right] + F_x^{(x)} + F_y^{(y)}. \tag{5.7a}$$

(Although represented symbolically, the term

$$\int_{-H}^{0} G\, dz = \frac{H^2}{2(1500\ \text{m s}^{-1})^2}$$

in the above.) It should be recognized that the surface pressure effect on density appears in the above terms containing G. Also, it is worth noting explicitly that the calculation of $\overline{\rho}$ in (5.7) departs from standard practice in that $\rho = \rho(S, T, p)$ is used. Solving the above elliptic equation for p_s completes the numerical calculation at a given time step.

b. A numerical example with an implicit time step

Dukowicz et al. (1993) discuss an implementation of the Bryan–Cox–Semtner ocean model for parallel computer architectures. This version uses a semi-implicit scheme for computing the Coriolis accelerations. Other time stepping techniques are standard; leapfrog time stepping is used for the advection parts of the problem and diffusive and viscous terms are lagged. Employing their approach here, the discrete (in time) form of (5.2) is

$$\begin{aligned} 0 = &-\left[\frac{1}{a\cos\theta}\frac{\partial}{\partial\phi} - \frac{f\delta t}{a}\frac{\partial}{\partial\theta}\right]\left[\left[H + \frac{gH^2}{2c_s^2}\right]p_{s\phi}\right] - \left[\frac{1}{a}\frac{\partial}{\partial\theta} + \frac{f\delta t}{a\cos\theta}\frac{\partial}{\partial\phi}\right]\left[\left[H + \frac{gH^2}{2c_s^2}\right]\cos\theta p_{s\theta}\right] \\ &+ f[\overline{V}^{-\phi} - (\overline{U}^{-}\cos\theta)_{\theta}] - \left[\frac{g}{a\cos\theta}\frac{\partial}{\partial\phi} - \frac{f\delta tg}{a}\frac{\partial}{\partial\theta}\right]\left[\int_{-H}^{0}\int_{0}^{z'}\overline{\rho}_{\phi}\, dz\, dz'\right] \\ &- \left[\frac{g}{a}\frac{\partial}{\partial\theta} - \frac{f\delta tg}{a\cos\theta}\frac{\partial}{\partial\phi}\right]\left[\cos\theta\int_{-H}^{0}\int_{0}^{z'}\overline{\rho}_{\theta}\, dz\, dz'\right] + \left[\frac{\partial}{\partial\phi} - f\delta t\frac{\partial}{\partial\theta}\cos\theta\right]HA^{\phi} + \left[\frac{\partial}{\partial\theta}\cos\theta + f\delta t\frac{\partial}{\partial\phi}\right]HA^{\theta}, \end{aligned} \tag{5.7b}$$

where $A^{(\phi,\theta)}$ represents the known advection and diffusion terms, $\overline{U}^{-}$ ($\overline{V}^{-}$) the vertically integrated zonal (meridional) velocity evaluated at the previous time step, δt the model time increment, and spherical coordinates have been used. The above is a generalization of Eq. (22) in Dukowicz et al. (1993) and, since the Coriolis accelerations remain unaffected by this change, is amenable to the operator splitting methods described therein.

c. Energetics consistency

An important constraint on the discretization employed in numerical models designed for long-term integrations is that they obey analytically based conservation principles. Among other things, this ensures that the models remain bounded in their behavior. One conservation principle, which experience has demonstrated as useful, involves the conversion between pressure work and gravitational potential energy. This is expressed analytically as

$$-\int \mathbf{u}\cdot\nabla p\, dV + \int \rho g w\, dV = 0, \tag{5.8}$$

and past models have employed discretizations in space, which insure that above integral constraint is met to machine precision (Bryan 1969; Semtner 1986; Dukowicz et al. 1993).

Here we emphasize that our proposed method for solving the hydrostatic equation and employing the real equation of state satisfies (5.8) for the specific spatial discretization (employing the nine-point stencil for the surface pressure equation) described in Dukowicz et al. (1993). Our arguments for this proceed identically to those presented in appendix A of Dukowicz et al., which demonstrates that the discrete representation of the pressure work done over all u, v cells can be written as

$$W = -a\sum h_{ijk}(u_{ijk}\delta_{\phi}\overline{p}^{\theta} + v_{ijk}\cos\theta\delta_{\theta}\overline{p}^{\phi})\Delta_{\theta}\Delta_{\phi}\Delta_{z}, \tag{5.9}$$

where a denotes the earth radius; i, j, k indices for the east, north, and vertical directions; $\delta_{\phi,\theta}$ discrete derivative operators; $\Delta_{\phi,\theta,z}$ grid spacings in the zonal, meridional, and vertical directions; h_{ijk} a domain boundary marker; an overbar $(\overline{\cdot})$ an averaging in the indicated direction; and the summation is over all model velocity cells. Straightforward manipulation of the finite-difference operators shows (5.9) can be rewritten as

$$W = a^2\sum h_{ijk}\delta_z p_{ijk}\cos\theta\Delta_{\theta}\Delta_{\phi}\Delta_{z}. \tag{5.10}$$

We recommend a Runge–Kutta integration of the hydrostatic equation, thus (5.8) is satisfied provided that we interpret the density in the hydrostatic equation as the RK averaged density; that is,

$$\overline{\rho} = \frac{\rho_1}{6} + \frac{\rho_2}{3} + \frac{\rho_3}{3} + \frac{\rho_4}{6},$$

where

$$\rho_1 = \rho(T_n, S_n, p_n),$$
$$\rho_2 = \rho(\overline{T}^z_n, \overline{S}^z_n, p_n + g\rho_1\Delta_z/2),$$
$$\rho_3 = \rho(\overline{T}^z_n, \overline{S}^z_n, p_n + g\rho_2\Delta_z/2),$$

and

$$\rho_4 = \rho(T_{n+1}, S_{n+1}, p_n + g\rho_3\Delta_z).$$

Subscripts n and $n + 1$ denote the vertical levels bounding the interval over which the vertical pressure gradient is to be estimated.

The native variables of a primitive equation model include T and S, from which P and ρ are diagnosed via the hydrostatic equation and the equation of state. Since it can be demonstrated that the advective terms do not contribute to the total kinetic energy (HKE), changes in HKE are thus governed by the net change in potential energy as measured in (5.9), and energy consistency in the sense of Bryan (1969) is demonstrated.

d. Free surface models

We now consider the modifications of a free surface model necessary to include the effects of total pressure in the equation of state. Following Killworth et al. (1991), (5.1d) is vertically integrated to yield

$$\eta_t + \left[\int_{-H}^{\eta} u\, dz\right]_x + \left[\int_{-H}^{\eta} v\, dz\right]_y = \eta_t + \overline{U}_x + \overline{V}_y = 0, \tag{5.11}$$

where η denotes the free surface, and $\overline{U}$ ($\overline{V}$) are the vertically integrated zonal and meridional velocities. [Note (5.11) neglects evaporation and precipitation. The inclusion of these effects in the free surface equation is discussed by Huang (1993).] Vertically integrating (5.1a,b) then returns

$$\rho_0\overline{U}_t = -\frac{\partial}{\partial x}\int_{-H}^{\eta} p\, dz + p(-H)H_x + \overline{F}^{(x)} \tag{5.12}$$

$$\rho_0\overline{V}_t = -\frac{\partial}{\partial y}\int_{-H}^{\eta} p\, dz + p(-H)H_y + \overline{F}^{(y)}, \tag{5.13}$$

where ρ_0 is an average fluid density, and the quantities $\overline{F}^{(x),(y)}$ represent inertial, Coriolis, and frictional effects; for example,

$$\overline{F}^{(x)} = -\frac{\partial}{\partial x}\int_{-H}^{\eta} uu\, dz - \frac{\partial}{\partial y}\int_{-H}^{\eta} uv\, dz + \int_{-H}^{\eta} (\text{frictional terms})\, dz + f\overline{V}.$$

Equations (5.11)–(5.13) form a set from which η can be predicted. The Killworth et al. (1991) procedure consists of breaking the model time steps into a sequence of short, barotropic intervals embedded in a longer baroclinic step. The quantities T and S are fixed over the barotropic steps, and (5.11)–(5.13) are used to predict a new free surface and barotropic velocity at the next baroclinic time level.

To include the effects of surface pressure on density in the above procedure, (5.6) is used in (5.12), (5.13) to evaluate both vertically integrated pressure and bottom pressure. After some algebra, these equations become

$$\rho_0\overline{U}_t = -\left[H + g\int_{-H}^{0} G\, dz\right]\frac{\partial}{\partial x}p_s - g\int_{-H}^{0}\int_{-z}^{0}\overline{\rho}_x\, dz'\, dz + \overline{F}^{(x)} \tag{5.14}$$

$$\rho_0\overline{V}_t = -\left[H + g\int_{-H}^{0} G\, dz\right]\frac{\partial}{\partial y}p_s - g\int_{-H}^{0}\int_{-z}^{0}\overline{\rho}_y\, dz'\, dz + \overline{F}^{(y)}, \tag{5.15}$$

where, again, the compressibility effect appears in the terms containing G and the calculation of $\overline{\rho}$. Equating p_s to $g\rho_0\eta$, as recommended by Killworth et al. (1991) closes the problem.

A natural question arises as to whether the G factors seriously affect the free surface evolution. Equivalently, one wonders if η may be predicted in the absence of the G factors in (5.14)–(5.15), and the resulting η used in the calculation of density at the next baroclinic time step. The size of these terms is

$$g\int_{-H}^{0} G\, dz \approx \frac{gH^2}{2c_s^2}. \tag{5.16}$$

Thus, the ratio of (5.13) to total fluid depth is

$$\frac{g\displaystyle\int_{-H}^{0} G\, dz}{H} \approx \frac{gH}{2c_s^2} \approx 0.01, \tag{5.17}$$

and their inclusion results in a modest few percent change in the outcome.

6. Conclusions

Considerations of the equation of state and hydrostatics leads us to conclude that the dynamical variations of pressure play a measurable role in the determination of density, and thus of baroclinic pressure gradients. Surface pressure gradients enhance internal pressure gradients in the same sense as those of the surface, and the enhancement grows in magnitude with depth. The transport associated with this baroclinic effect of dynamically varying pressure can be several Sverdrups and the associated velocities can be several cm s^{-1} for Gulf Stream–like conditions. Further, we have outlined

procedures by which rigid lid and free surface models can account for this effect.

It is worth emphasizing that our estimates indicate net transport is affected by the present feedback between total pressure and density. The impact this may have on model results is not currently known, but because transports are of particular importance to climate, we recommend that such models include the real equation of state when solving the hydrostatic equation. On the other hand, global heat and salt transports reflect surface exchanges of buoyancy between the ocean and atmosphere, and these are likely to be unaffected by the enhanced transports suggested herein. Hence, the above feedback might well be confined to local modifications of model output. Comparisons of models with and without the proper form of the hydrostatic equation will serve to clarify this point.

Acknowledgments. The authors would like to thank Katherine White, Anne de Miranda, Jochem Marotzke, and Frank Bryan for informative discussions. Two anonymous referees also provided penetrating reviews. WKD is supported by NSF Grant OCE-9401977 and NASA Grants NAGW-3087 and NAGW-4883. YH and DY are supported by NSF Grant OCE-9115365, ONR Contract N00014-95-1-0501, and MMS Cooperative Agreement 14-35-0001-30804. Ms. Sheila Heseltine prepared the manuscript and the final figures and Ms. Jane Jimeian helped with computational parts of the paper.

REFERENCES

Bryan, K., 1969: A numerical method for the study of the circulation of the World Ocean. *J. Comput. Phys.,* **4,** 347–376.

Dickson, R. R., E. M. Gmitrowisz, and A. J. Watson, 1990: Deep-water renewal in the northern North Atlantic. *Nature,* **344,** 848–850.

Dukowicz, J., and R. Smith, 1994: Implicit free surface method for the Bryan–Cox–Semtner ocean model. *J. Geophys. Res.,* **99,** 7991–8014.

——, ——, and R. Malone, 1993: A reformulation and implementation of the Bryan–Cox–Semtner model on the connection machine. *J. Atmos. Oceanic Technol.,* **10,** 195–208.

Feistel, R., 1993: Equilibrium thermodynamics of seawater revisited. *Progress in Oceanography,* Vol. 31, Pergamon, 101–179.

——, and E. Hagen, 1995: On the Gibbs thermodynamic potential of seawater. *Progress in Oceanography,* Vol. 36, Pergamon, 249–327.

Fofonoff, N. P., and R. C. Millard Jr., 1983: Algorithms for computation of fundamental properties of seawater. Tech. Paper Mar. Sci. 44, UNESCO, 53 pp. [Available from Division of Marine Sciences, UNESCO, Place de Fonenoy, 75700 Paris, France.]

Gill, A., 1982: *Atmosphere–Ocean Dynamics.* Academic Press, 662 pp.

Hsueh, Y., 1997: The Kuroshio in the East China Sea. *J. Mar. Syst.,* in press.

——, J. Schultz, and W. Holland, 1997: The Kuroshio flow-through in the East China Sea: A numerical model. *Progress in Oceanography,* in press.

Huang, R. X., 1993: Real freshwater flux as a natural boundary condition for the salinity balance and thermohaline circulation forced by evaporation and precipitation. *J. Phys. Oceanogr.,* **23,** 2428–2446.

Jackett, D. R., and T. J. McDougall, 1995: Minimal adjustment of hydrographic profiles to achieve statric stability. *J. Atmos. Oceanic Technol.,* **12,** 381–389.

Killworth, P. D., D. Stainforth, D. J. Webb, and S. M. Paterson, 1991: The development of a free surface Bryan–Cox–Semtner model. *J. Phys. Oceanogr.,* **21,** 1333–1348.

Levitus, S., 1982: *Climatological Atlas of the World Ocean.* NOAA Prof. Paper No. 13, U. S. Govt. Printing Office, 173 pp.

——, R. Burgert, and T. P. Boyer, 1994a: *World Ocean Atlas.* Vol. 3: *Salinity.* U. S. Department of Commerce, NOAA, 99 pp.

——, ——, and ——, 1994b: *World Ocean Atlas.* Vol. 4: *Temperature.* U. S. Department of Commerce, NOAA, 117 pp.

Millero, F. J., C.-T. Chen, A. Bradshaw, and K. Schleicher, 1980: A new high pressure equation of state for seawater. *Deep-Sea Res.,* **27A,** 255–264.

Rossby, T., 1984: On the energetics of the Gulf Stream at 73W. *J. Mar. Res.,* **45,** 59–82.

Schultz, J., 1994: A numerical model of the Kuroshio in the East China Sea. Ph.D. dissertation, The Florida State University, 144 pp. [Available from DIRAC Library, The Florida State University, Tallahassee, FL 32306.]

Semtner, A., Jr., 1986: Finite-difference formulation of a World Ocean model. *Advanced Physical Oceanographic Numerical Modelling,* J. O'Brien Ed., D. Reidel, 187–202.

WOCE Operations Manual, 1994: WHP Office Rep. 90–1, May, Rev. 2, WOCE Rep. No. 67/91, 144 pp. [Available from J. Kappa, UCSD/S10, WOCE Hydrographic Program Office, 9500 Gilman Drive 0214, NORPAX, Rm. 316, La Jolla, CA 92093-0214.]